Received: 4 October 2023 | Revised: 15 April 2024 | Accepted: 17 April 2024

DOI: 10.1002/esp.5868

RESEARCH ARTICLE

ESPL WILEY

Debris-flow entrainment modelling under climate change: Considering antecedent moisture conditions along the flow path

Anna Lena Könz[1,2] | Jacob Hirschberg[1,3] | Brian W. McArdell[1] | Benjamin B. Mirus[1,4] | Tjalling de Haas[5] | Perry Bartelt[6] | Peter Molnar[2]

[1]Swiss Federal Institute for Forest, Snow and Landscape Research WSL, Birmensdorf, Switzerland

[2]Institute of Environmental Engineering, ETH Zurich, Zurich, Switzerland

[3]Geological Institute, ETH Zurich, Zurich, Switzerland

[4]U.S. Geological Survey, Geological Hazards Science Center, Golden, Colorado, USA

[5]Department of Physical Geography, Utrecht University, Utrecht, The Netherlands

[6]WSL Institute for Snow and Avalanche Research SLF, Davos, Switzerland

Correspondence
Anna Lena Könz, Swiss Federal Institute for Forest, Snow and Landscape Research WSL, Birmensdorf, Switzerland.
Email: anna.koenz@wsl.ch

Jacob Hirschberg, Geological Institute, ETH Zurich, Zurich, Switzerland.
Email: jacob.hirschberg@erdw.ethz.ch

Funding information
Climate Change Impacts on Alpine Mass Movements (CCAMM)

Abstract

Debris-flow volumes can increase along their flow path by entraining sediment stored in the channel bed and banks, thus also increasing hazard potential. Theoretical considerations, laboratory experiments and field investigations all indicate that the saturation conditions of the sediment along the flow path can greatly influence the amount of sediment entrained. However, this process is usually not considered for practical applications. This study aims to close this gap by combining runout and hydrological models into a predictive framework that is calibrated and tested using unique observations of sediment erosion and debris-flow properties available at a Swiss debris-flow observation station (Illgraben). To this end, hourly water input to the erodible channel is predicted using a simple, process-based hydrological model, and the resulting water saturation level in the upper sediment layer of the channel is modelled based on a Hortonian infiltration concept. Debris-flow entrainment is then predicted using the RAMMS debris-flow runout model. We find a strong correlation between the modelled saturation level of the sediment on the flow path and the channel-bed erodibility for single-surge debris-flow events with distinct fronts, indicating that the modelled water content is a good predictor for erosion simulated in RAMMS. Debris-flow properties with more complex flow behaviour (e.g., multiple surges or roll waves) are not as well predicted using this procedure, indicating that more physically complete models are necessary. Finally, we demonstrate how this modelling framework can be used for climate change impact assessment and show that earlier snowmelt may shift the peak of the debris-flow season to earlier in the year. Our novel modelling framework provides a plausible approach to reproduce saturation-dependent entrainment and thus better constrain event volumes for current and future hazard assessment.

KEYWORDS
antecedent saturation conditions, climate change, debris flows, entrainment, infiltration, modelling, RAMMS, revised Horton infiltration model

1 | INTRODUCTION

Debris flows are a type of landslide and a natural hazard posing severe risks in mountain areas (Badoux et al., 2016; Dowling & Santi, 2014). In a warming climate, changes in rainfall patterns and sediment availability are expected to also affect debris-flow dynamics. Future debris-flow frequency may increase, decrease or shift in seasonality (Gariano & Guzzetti, 2016; Hirschberg et al., 2021; Kaitna et al., 2023), while changes in debris-flow volume, associated runout and risk have yet to be identified. Thus, an understanding of the physical processes governing the evolution of debris flows and their effect on local communities and

infrastructure is crucial for the prediction of hazards today and in the future.

The expected debris-flow volume is an important input to debris-flow runout models for the delineation of affected areas and the design of mitigation structures (i.e., retention basins Prochaska et al., 2008). Although initial volumes may be small, bank collapse, channel erosion and subsequent entrainment of the eroded sediment into the debris flow can increase the mobilized volume by several orders of magnitude (Jakob & Hungr, 2005). Thus, the efficiency of the entrainment process, which can vary substantially between sites and individual events (de Haas et al., 2022; Frank et al.2017), is a strong predictor of the total debris-flow magnitude (Jakob & Hungr, 2005). This relevant volume increase due to entrainment occurs not only in steep channel sections but also in downstream lower gradient fan areas (Berger et al., 2011; de Haas et al., 2020; Schürch et al.2011).

Theoretical considerations, laboratory experiments and field observations have shown positive correlations between wet channel-bed conditions and eroded volumes (Iverson et al., 2011; McCoy et al., 2012; Sassa & Wang, 2005). The undrained loading imposed by debris-flow masses induces elevated pore-water pressures within the torrent deposits, reducing basal friction and leading to pronounced flow-momentum growth (Iverson et al., 2011). If the increased pore-water pressure is accompanied by volume contraction (e.g., through the collapse of soil structure or grain crushing), bed liquefaction can further increase bed erodibility (Roelofs et al., 2023; Sassa & Wang, 2005; Zheng et al., 2023). These phenomena are not confined solely to debris flows, but extend to other types of landslides, such as rock avalanches (Aaron & McDougall, 2019), as well as to mass-wasting process transitions (e.g., shallow landslide or rock avalanche to debris flow). This became apparent in the catastrophic 2017 rock-slope failure at Pizzo Cengalo (Switzerland), which developed into a rock avalanche and the subsequent release of multiple debris-flow surges (Walter et al., 2020). The entrainment of water-saturated sediments is thought to be the pivotal factor for initiating these hazardous debris flows.

Although the importance of bed saturation level in debris-flow dynamics has been established, the mechanics of the entrainment process remain poorly constrained. Nevertheless, the consideration of saturation conditions in hazard assessment could prove highly beneficial. This is particularly true for future hazard prediction, as climate change is expected to not only affect the rainfall conditions for run-off-triggered debris flows but also the antecedent moisture conditions along the flow paths (Hirschberg et al., 2021; Kaitna et al., 2023).

To analyse the risks associated with debris-flow activity, numerical modelling of the flow propagation, and in particular the runout behaviour, plays an important role in practical applications such as hazard mapping, mitigation strategies and land use planning. Several physically based numerical models have been developed for this purpose (e.g., Christen et al., 2010; Hungr & McDougall, 2009), primarily focused on the reproduction of flow properties and runout patterns, while typically ignoring entrainment. In recent years, different attempts to include the entrainment process in runout models have improved modelled flow properties and runout behaviour by empirically correlating entrainment volumes to individual flow properties (e.g., Frank et al., 2015; Hussin et al., 2012; Reid et al., 2016). The application of these models to different study areas has resulted in accurate reproductions of flow velocities, entrainment volumes and runout patterns (Baggio et al.2021; Dietrich & Krautblatter, 2019; Frank et al., 2017; Lee et al., 2022). However, methods for predicting entrainment based on environmental factors such as channel-bed wetness are missing.

Here, we aim to test a novel sequentially coupled modelling chain, including a channel-bed erodibility estimation based on flow-path saturation level, on a unique dataset of debris-flow events and erosion on the Illgraben alluvial fan (Switzerland). To this end, the modified RApid Mass Movements Simulation (RAMMS) runout model as proposed by Frank et al. (2015) is used to simulate debris-flow dynamics. The model includes a shear stress dependent entrainment module, with its primary calibration parameter $dz/d\tau$ describing channel-bed erodibility (i.e., susceptibility of the bed material to be eroded). Erodibility is determined by the bed's resisting forces, and as such, it is assumed to be independent of an event's erosivity (i.e., the debris-flow's potential to cause erosion). The bed saturation level (defined as the volumetric water content divided by pore space) is predicted using a water balance model covering the period of 2019–2022.

The proposed modelling framework is used to (i) test the reproduction of flow properties and erosion patterns modelled in RAMMS, (ii) enable a prediction of expected channel-bed erodibility based on modelled flow-path water content and (iii) assess future channel-bed conditions by forcing the hydrological model with climate change scenarios.

2 | METHODS

2.1 | The Illgraben study site

The Illgraben basin (9.0 km^2) is situated in the Swiss Rhône Valley. It features a steep terrain descending from the Illhorn summit (2716 m a.s.l.), transitioning into a more gradual incline (approx. 10% to 8% McArdell et al., 2007) across the large alluvial fan (apex at 850 m a.s.l.) down to the confluence of the Illgraben torrent and the Rhône River (610 m a.s.l., Figure 1 Hürlimann et al., 2003). With a debris-flow occurrence of two to eight events per year, the Illgraben is one of the most active Alpine debris-flow basins (Hirschberg et al., 2021). The headwaters of the Illgraben torrent can be divided into two subcatchments (Figure 1a). The eastern Illbach subcatchment shows little to no run-off and is not susceptible to debris flows (Hirschberg et al., 2021). Thus, in this study, only the geomorphologically active Illgraben subcatchment (4.8 km^2) is considered. The Illgraben torrent flows through a 4.8-km-long incised channel with an unconsolidated bed, which has been stabilized with about 30 check dams (Lichtenhahn, 1971). The lower channel reach is an ephemeral stream with continuous run-off occurring only during the snowmelt season from March to May (Hirschberg et al.2019).

Relevant flow properties such as flow depth, normal and shear forces, as well as vibration (geophone, accelerometers), are measured at Check Dam 29 (CD29, Figure 1). From 2019 to 2022, key flow variables such as maximum flow depths, frontal flow velocities, mean bulk densities and total flow volumes are published for all recorded events (McArdell et al., 2023), enabling the computation of maximum shear stress and the flow's Froude number (Table 1). Soil moisture sensors (SM28) have been installed on the channel bank at CD28 since 6 June 2022, and photographs of the channel bed are available at hourly

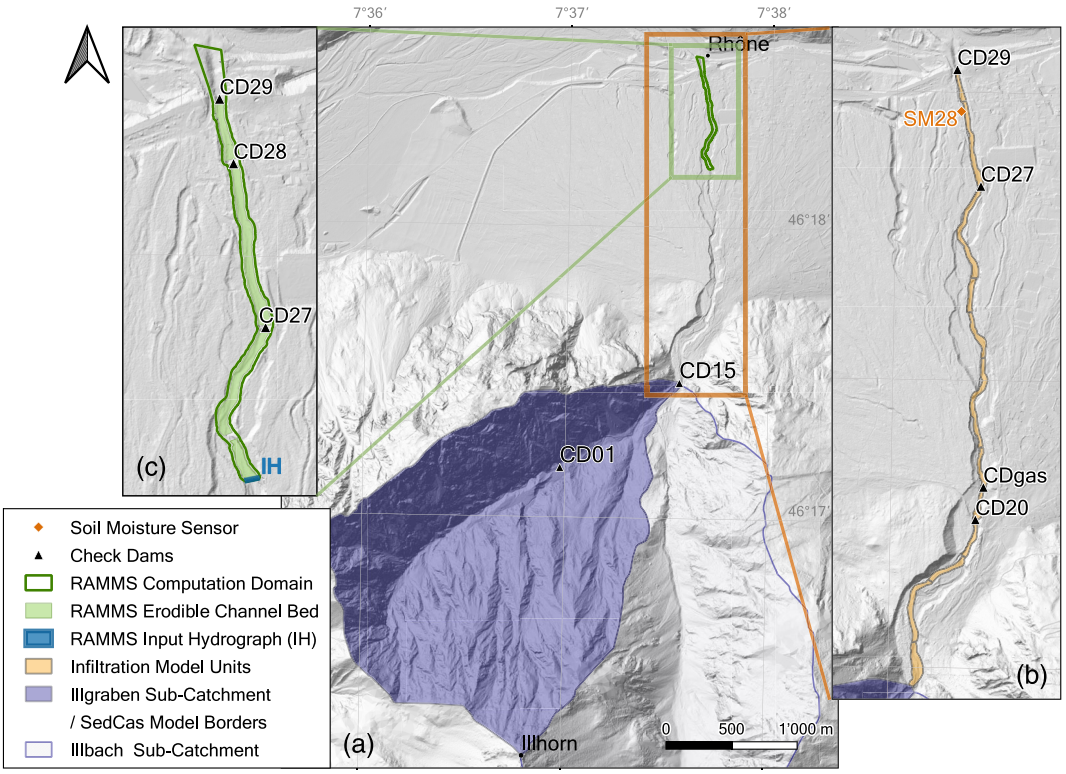

FIGURE 1 Overview of study site at Illgraben (Switzerland) with the domains considered for (a) the modified SedCas model providing discharge to the Illgraben channel on the fan, (b) the single channel units used for the InfChan model and (c) for the RAMMS debris-flow runout modelling, as well as the locations of relevant measurement sites. The shaded relief map is provided by the Federal Office of Topography Swisstopo. [Color figure can be viewed at wileyonlinelibrary.com]

intervals for locations CD01, CDgas, CD27 and CD29, with irregular coverage extending from 2019 to 2022 (as detailed in Appendix A.4 in the Supporting Information). Additionally, de Haas et al. (2022) published a set of high-quality digital surface models (DSMs) of the channel below the apex, generated with structure-from-motion photogrammetry. DSMs are generated regularly from 2019 to 2022 between debris-flow events, yielding in DSM of difference (DoD) for most events. Long-term meteorological data (i.e., precipitation, temperature and incoming shortwave radiation) were retrieved from the Swiss Federal Office of Meteorology and Climatology (MeteoSwiss) station located in Montana (1423 m a.s.l.), approximately 11 km west of Illgraben.

2.2 | Debris-flow entrainment modelling

The RAMMS debris-flow simulation software is widely used in both research and practice (Dietrich & Krautblatter, 2019; Frank et al., 2015) to calculate flow properties and runout over three-dimensional terrain (Bartelt et al., 2013). It solves the two-dimensional depth-averaged shallow water equations and a Voellmy-fluid friction model, where frictional resistance is divided into a dry Coulomb-type friction μ (scaled with flow depth) and a viscous-turbulent friction ξ (scaled with flow velocity Bartelt et al., 2013; Christen et al., 2010). The erosion module in RAMMS predicts the net decrease in bed elevation resulting from the entrainment of sediment from the bed as a function of maximum shear stress (Bartelt et al., 2013). The shear stress τ acting on the channel bed is predicted by RAMMS for each cell on the computational grid. The maximum potential erosion depth e_m is defined as follows:

$$e_m = \begin{cases} 0 & \tau < \tau_c, \\ \dfrac{dz}{d\tau}(\tau_{\max} - \tau_c) & \tau \geq \tau_c, \end{cases} \quad (1)$$

with the erosion proportionality factor $dz/d\tau$ linking erosion depth to shear stress exerted on the channel bed (referred to as bed erodibility). Starting from when the critical shear stress τ_c is exceeded and lasting until the actual erosion depth e_t reaches the maximum potential erosion depth e_m, the model entrains sediment at a constant erosion rate dz/dt. The maximum potential erosion depth is updated when the maximum bed shear stress ($\tau_{\max}$) increases during the simulation (Frank et al., 2015).

This entrainment model uses a generalized empirical relationship based on field data from Schürch et al. (2011) and has been demonstrated to yield reasonable results (e.g., Lee et al., 2022). As described in Equation (1), it predicts that the maximum depth of erosion is related to the maximum shear stress in the debris flow, usually at the flow front. Although this was not investigated by Frank et al. (2015), it is plausible that other processes, such as granular agitation and large fluid pore pressure, promote infiltration of water into the channel bed, resulting in a reduction of the shear resistance and thereby enhancing erosion of sediment. Sediment grain size is not explicitly included in the RAMMS model.

Here, RAMMS was used to compute the erosive behaviour of seven well-documented debris-flow events, recorded from 2019 to

TABLE 1 Summary of debris-flow characteristics (maximum flow depth h_{max}, maximum shear stress τ_{max}, frontal Froude number *Fr*, observed erodibility $dz/d\tau_{obs}$) and eroded volumes (V_{eroded}) observed for all 16 debris-flow events (2019–2022), along with simulated debris-flow properties and calibrated parameters (viscous-turbulent friction ξ, erodibility parameter $dz/d\tau_{cal}$) for the seven erosive events considered in RAMMS.

ID	Date	ξ *cal* (m/s^2)	$\frac{dz}{d\tau_{cal}}$ *cal* (m/kPa)	h_{max} *obs* (m)	*sim* (m)	V_{eroded} *obs* (m^3)	*sim* (m^3)	τ_{max} *obs* (kPa)	*Fr* *obs* (-)	$\frac{dz}{d\tau_{obs}} = -\frac{dz}{\tau_{max}}$ *obs* (m/kPa)
1	21.06.2019	4500[c]	0.10	2.7	2.8	−1297.5	−1274.9	3.67	1.65	0.44
2	15.07.2019			0.7		136.1		1.16	1.59	−0.15
3	26.07.2019	8000	0.24	1.4	1.4	−1432.0	−1374.6	2.01	3.11	0.89
4	11.08.2019	8500[c]	0.09	1.9	1.7	−561.9	−595.3	2.64	1.99	0.27
5	20.08.2019			1.1		−218.2		1.62	0.46	0.17
6	29.06.2020			1.2		121.2		1.61	0.43	−0.09
7	17.08.2020			0.7		2137.7		0.94	0.30	−2.83
8	30.08.2020			1.9		−5665.2		2.36	2.35[b]	3.01
9	05.06.2021			0.5		−581.3		0.46	1.29	1.57
10	06.07.2021	4000	0.08	2.6	2.7	−1120.4	−1119.0	3.01	2.20	0.46
11	16.07.2021			2.4		2165.8		3.29	0.84	−0.82
12	07.08.2021	230[c]	0.08	1.6[a]	1.5	−666.8	−661.1	2.85	0.74	0.29
13	19.09.2021	160[c]	0.10	1.2	0.8	−262.7	−269.1	1.46	0.47	0.22
14	05.06.2022			2.2		1365.6		2.30	1.14	−0.74
15	04.07.2022	9000	0.15	2.6	2.5	−1645.2	−1676.7	2.72	2.07	0.76
16	08.09.2022			1.8		1124.1		1.93	0.56	−0.73

Note: In RAMMS, the Coulomb friction parameter was set to $\mu = 0.06$ for all events.

[a]Minor changes were made to the original dataset following a detailed examination of the observations: The maximum flow depth was reduced to the maximum computed moving average.

[b]Minor changes were made to the original dataset following a detailed examination of the observations: The peak velocity of the first peak was interchanged with the velocity of the second, faster peak.

[c]ξ-values were calibrated by Bolliger et al. (2024).

2022 (Table 1). The calibration only comprised events that allowed for the effective constraint of bed erodilibility using RAMMS. Thus, events displaying depositional character or featuring complex hydrograph patterns (e.g., multiple surges) were excluded.

The spatial information required by RAMMS, including the pre-event digital elevation models (DEMs), the extent of the calculation domain and the boundaries of the erodible channel bed (Figure 1c), were obtained from the study conducted by de Haas et al. (2022). The check dams were considered as non-eroding cells within the erodible bed. To optimize the simulation runtime and numerical stability, we used a 0.5-m resolution grid, which was smoothed with a moving average window of 2.5 m (i.e., 25% of the channel width) to eliminate microtopography (as recommended by Baggio et al., 2021; Lee et al., 2022). The input hydrograph at the upstream boundary of the simulation domain was approximated from high-resolution measurements of flow depth obtained at the force plate location (CD29, Fig 1c).

The calibration of the RAMMS model largely followed the procedure outlined in the user manual (Bartelt et al., 2013). First, the model was calibrated to best-fit maximum flow depth and frontal flow velocity, without considering entrainment. This preliminary calibration helped to narrow down the choice of the friction parameters (μ and ξ, building on Bolliger et al., 2024). Second, the calibration was repeated considering erosion. The Coulomb friction parameter was held at a constant value of $\mu = 0.06$, corresponding approximately to the channel slope within the modelling domain (Bartelt et al., 2013; Frank et al., 2017), and yielding the best results in the entrainment-free calibration. Most erosion-related parameters were maintained at default values, with $dz/dt = -0.025\,m\,s^{-1}$ and $\tau_{crit} = 1\,kPa$, derived from observations at Illgraben (Berger et al., 2011; Frank et al., 2015). Consequently, the calibration parameters were effectively reduced to two key components: (i) the viscous-turbulent friction parameter ξ, fine-tuned to achieve the expected maximum flow depths (Table 1), frontal velocities (Appendix A.1, Table A1 in the Supporting Information) and overall hydrograph character (visual assessment, refer to Figure 2), as well as (ii) the erodibility parameter $dz/d\tau$, which was calibrated to match the observed eroded volumes (Table 1). The calibrated parameter $dz/d\tau_{cal}$ was used as an indicator for channel-bed erodibility in the subsequent analysis.

2.3 | Channel-bed water balance modelling

For estimating the water discharge from the headwaters entering the lower channel reaches downstream from the fan apex, we used the hydrological module of the geomorphic sediment cascade model (SedCas Bennett et al., 2014; Hirschberg et al., 2021). SedCas solves the water balance for connected linear reservoirs that represent hydrological response units (HRUs). It was originally calibrated for Illgraben including first-order processes of sediment production and debris-flow triggering (Hirschberg et al., 2021). Here, two substantial changes were made to the original model code: (i) rather than solving the water balance for lumped HRUs (vegetated and non-vegetated) the Illgraben catchment was further discretized in elevation bands of 100 m vertical length, which improves the representation of

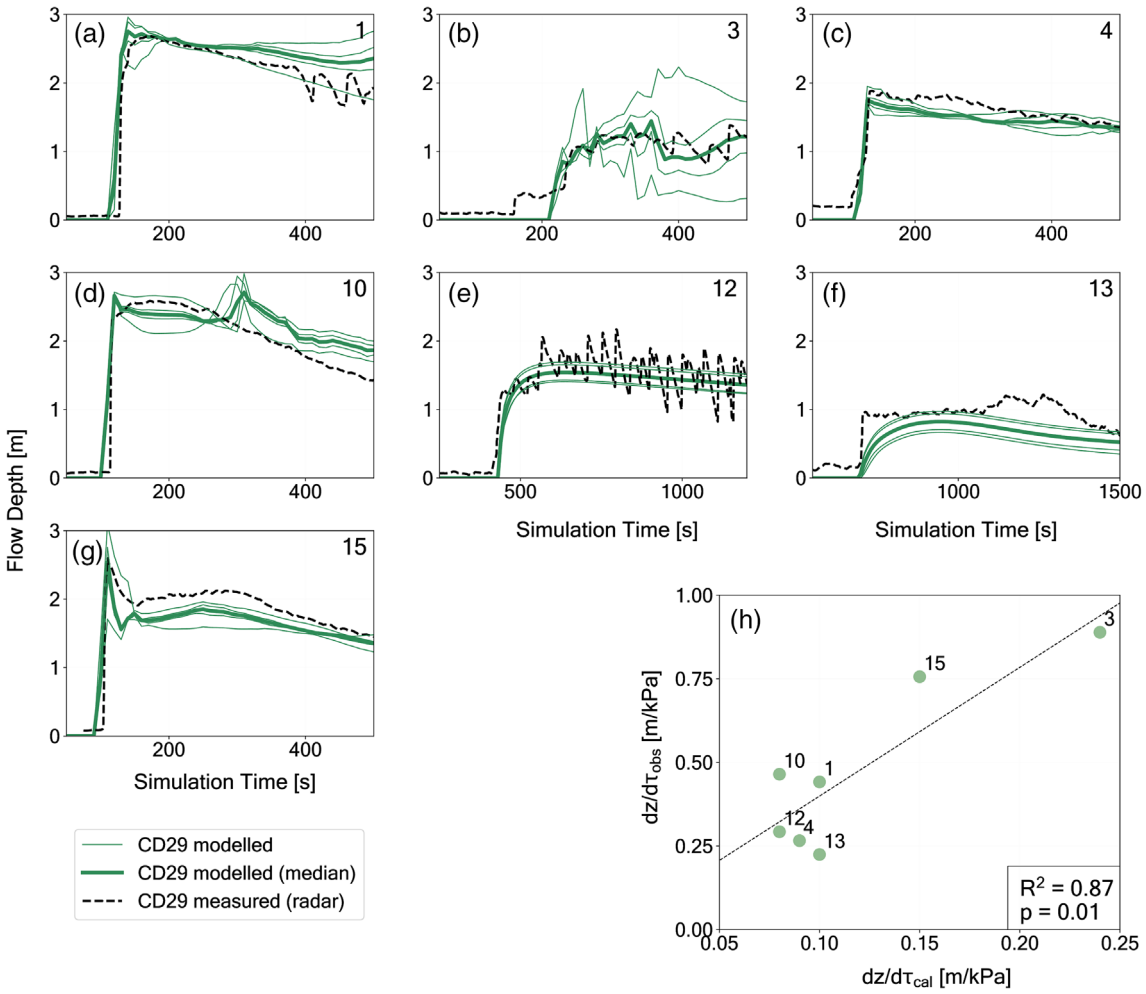

FIGURE 2 RAMMS result representation of (a)–(g) modelled and measured hydrographs at CD29 (Figure 1) from the catalogue of RAMMS-calibrated debris-flow events. The event ID corresponds to the chronological order of all 16 recorded events (Table 1). The measured data are retrieved from max. front flow depth measured with the radar at CD29 (McArdell, 2016). The modelled data are plotted at four points along the CD29 cross-section (thin green lines) and as its median (bold green line). The calibrated erodibility ($dz/d\tau_{cal}$) vs. observed erodibility ($dz/d\tau_{obs}$) comparison is shown in (h). The numbers indicate the event ID, the black dotted line represents the linear regression of the data points and the coefficient of determination (R^2) and p values show the results of the Pearson correlation test (using *scipy.stats.pearsonr*-function). Please note that $dz/d\tau_{cal}$ and $dz/d\tau_{obs}$ are not equivalent variables (Section 3.1). [Color figure can be viewed at wileyonlinelibrary.com]

temperature-dependent processes like snow accumulation and melt; (ii) a Horton infiltration model (InfChan) was coupled with the existing model to estimate infiltration losses along the flow path on the fan and the resulting moisture conditions in the lower channel reaches (Figure 1b). To this end, the modified Horton infiltration (MHI) algorithm (Wang & Chu, 2020) was applied.

In MHI, the originally event-based Horton equation is redefined such that it can be applied in a continuous model (Horton, 1939). Horton describes the potential infiltration capacity f_p at a given time t, with f_c (mm/h) as the final equilibrium infiltration capacity, f_0 (mm/h) as the initial infiltration capacity and k as an empirical decay parameter (1/h), modelling the reduction in infiltration capacity as the soil becomes progressively saturated during rainfall.

$$f_p(t) = f_c + (f_0 - f_c)e^{-kt}. \quad (2)$$

Extending the model from event-based to continuous requires a description for the recovery of the infiltration capacity in dry periods. To this end, time t is replaced by cumulative infiltration (in mm, defined as the integration of the infiltration capacity f_p in mm/h over a given duration in h) as a proxy for soil water content at a given time. This allows for changes in soil water content to directly influence the soil's infiltration capacity. The wetting process of the soil is controlled by a volumetric water-content threshold (%), the field capacity threshold (*FC*), at which water in larger pores has been gravitationally drained away. The relationship between infiltration and storage exhibits linear behaviour for soil wetted beyond *FC* and fast non-linear behaviour for soil storage below *FC*. Soil drying through drainage and evaporation is influenced by a soil moisture threshold as well, with the recovery process being primarily driven by gravitational drainage when the soil's storage exceeds *FC*. Below *FC* and until the soil's wilting point (*WP*) is reached, soil drying is solely influenced by evaporation. The resulting run-off from a single model unit is generated by rainfall exceeding the infiltration capacity $f_p(t)$ of the top soil layer (infiltration excess) as well as when the maximum soil water storage capacity M_{max} (mm) is reached (saturation excess). Thus, based on climate data and soil properties, the MHI algorithm enables the partitioning of the incoming flow into evaporation, water stored in the

TABLE 2 Overview of the InfChan model parameters (M_{max}: maximum soil water storage, k: decay constant, f_c: final equilibrium infiltration capacity, *WP*: wilting point, *FC*: field capacity, *WS*: saturated water content).

	M_{max} (mm)	k (h^{-1})	f_c (mm h^{-1})	*WP* (-)	*FC* (-)	*WS* (-)
Considered ranges	50–2500	0.005–0.5	0.5–20.0	-	-	-
Applied model parameters	1400	0.1/0.2/0.5	5.0	0.05	0.15	0.45
Literature	-	0.4[d]	0.6–6.0[a,b,c]	0.06[c]	0.14[c]	0.43[c]

Note: The ranges considered in the model calibration, the final model parameters and their literature values are listed.
[a]Meijer (2019).
[b]Rossman and Huber (2016).
[c]C. (1933).
[d]Wang and Chu (2020).

bed material, deep percolation and surface run-off to downstream channel reaches. For a full description of the MHI algorithm, the reader is referred to Wang and Chu (2020).

For translating the MHI algorithm into a channel infiltration model (InfChan), the channel section of the Illgraben fan, reaching from the fan apex (CD15) to the force plate (CD29, Figure 1b), was partitioned into 12 HRUs of roughly 200 m in length, corresponding to the mobile channel bed between check dams. The MHI algorithm was applied to each HRU at an hourly resolution, and with the only connection being the transfer of surface run-off generated within a given HRU as surface inflow to the next HRU downstream. InfChan was forced with the modelled headwater discharge and the same meteorological data as for the SedCas hydrological module.

Due to limited data availability on hydrological conditions in the Illgraben fan area, and especially within the torrent channel, a straightforward definition of calibration criteria was not possible. Thus, we used multiple lines of evidence to constrain the InfChan model parametrization. The model's performance in reproducing subsurface processes was captured by comparing the modelled saturation level to the soil moisture data measured in the channel bank (Figure 1b, SM28). The performance was quantified in terms of (i) the drying rate of the soil (as fitted decay parameter of the soil water-content time series) and (ii) the model accuracy in reproducing different degrees of saturation over the measured time period (based on a confusion matrix as described by Fawcett, 2006). Surface flow conditions in the channel bed were considered by building a catalogue of hourly high flow, low flow and dry channel-bed conditions. Similar to the flow category scale devised by Quinlan et al. (2015), the catalogue was based on hourly channel photographs for different locations along the channel (Appendix A.4 in the Supporting Information). The modelled flow behaviour was analogously classified into the three flow conditions, which enabled the comparison to the observed categories with regard to (iii) daily model accuracy (defined analogously to the accuracy of soil saturation level), as well as (iv) spatial and (v) seasonal statistics reproduction (based on cumulative hours of high flow, low flow and dry channel-bed conditions at the different locations and for different months respectively). The five resulting performance metrics were merged into a combined calibration criterion. For a more detailed metric description refer to Appendix A.3 in the Supporting Information.

The MHI algorithm by Wang and Chu (2020), described in earlier paragraphs, requires six soil-specific model parameters: f_c, k, M_{max}, WS, FC and *WP*. Based on literature values (C., 1933; Meijer, 2019; Rossman & Huber, 2016; Wang & Chu, 2020) and soil moisture data (SM28, Figure 1b), an initial set of parameter values was defined (Table 2). To calibrate the model towards reproducing the observed hydrological characteristics (surface and subsurface), only two parameters were considered (f_c and k). For these two calibration parameters, 49 (7×7) possible parameter combinations within a meaningful physical range were implemented. The performance of each simulation was quantified based on the aforementioned combined calibration criteria (refer to Appendix A.3 in the Supporting Information). The remaining parameters were kept at literature values (WS, FC and *WP*, Table 2) or specified in a later step (i.e., M_{max} in Section 2.4).

2.4 | Linking RAMMS with modelled channel water content

The RAMMS and hydrological modelling yielded two datasets: (i) the RAMMS-derived calibrated bed erodibility $dz/d\tau_{cal}$ linked to specific debris-flow occurrence and (ii) a long-term time series of channel-bed saturation conditions in the lower channel reaches, within the RAMMS modelling domain. The two datasets were combined by considering the moisture conditions prior to the debris-flow front arrival and linking it to the corresponding event's $dz/d\tau_{cal}$. To determine the storage volume that governs antecedent channel-bed wetting, we assessed the ability of the InfChan model output to predict channel-bed erodibility most effectively depending on the selected M_{max} value. For this purpose, the hydrological calibration (as outlined in Section 2.3) was repeated for varying M_{max} values (Table 2) and optimized for the highest correlation between pre-event saturation level and $dz/d\tau_{cal}$ values.

The resulting field-derived set of erodibility-saturation pairs was expanded by incorporating a similar dataset obtained from large-scale flume experiments conducted by Iverson et al. (2011). In this regard, we calibrated the erodibility parameter $dz/d\tau_{cal}$ through a series of entrainment experiments, with the experimental flume featuring an erodible bed with pre-established varying antecedent water contents (Appendix A.2 in the Supporting Information). Additionally, to expand the dataset of field observations, all the 16 well-documented debris-flow events recorded at Illgraben between 2019 and 2022 (Table 1), were included by introducing the observed event erodibility $dz/d\tau_{obs}$. It was defined as the negative recorded erosion depth divided by maximum measured shear stress ($-dz/\tau_{max}$) and could also be correlated with the pre-event modelled saturation level.

To identify potential driving mechanisms of erodibility beyond water content of the channel bed, further measurements available for the Illgraben site were considered (Table 1 and Appendix A.1, Table A1 in the Supporting Information). Additional parameters included antecedent rain sums (from the MeteoSwiss time series), debris-flow frontal Froude number, mean debris-flow bulk density and total flow volume (based on data measured at CD29 McArdell et al., 2023), as well as sediment availability in the channel (approximated with the mean channel elevation of the pre-event DEM). Furthermore, to accommodate more complex flow phenomena that were not mirrored in the characteristic parameters of the event, the complete event catalogue was classified into four event categories (steep-front events, gradual-front events, multi-surge events and events exhibiting roll waves, Appendix A.1, Figure A1 in the Supporting Information) based on the hydrographs measured at CD29 in combination with video footage of the events.

2.5 | Climate change impact assessment on debris-flow entrainment

Given that channel-bed saturation level can be used as a proxy for channel-bed erodibility, the calibrated InfChan model allows for an investigation of future climate change impacts on saturation conditions and thus on the entrainment process. To this end, the presented hydrological modelling framework is forced with the same climate change scenarios used by Hirschberg et al. (2021) for the climate change impact assessment of debris-flow triggering. The stochastic Advanced WEather GENerator (AWE-GEN) (Fatichi et al., 2011), calibrated against the nearest MeteoSwiss station of Montana, was used to produce hourly climate variable time series for 30 years representative of historical (1981–2010) and future periods. For the future periods, centred around 2035, 2060 and 2085, climatic factors of change were derived for the most extreme emission forcing (RCP8.5) included in the CH2018 climate scenarios, a debiased version of the EURO-CORDEX ensemble of climate simulations with regional climate models (CH2018, 2018). For each future period, 31 sets of factors of change are considered, representing the uncertainty within the RCP8.5 scenario. For each new parameter set, 50 stochastic realizations over 30 years are included in the ensemble. For further details on the generation of the future climate data, refer to Hirschberg et al. (2021).

The long-term monthly median of modelled saturation level in the lower channel reaches (HRU12) is compared for present and future climates. Furthermore, monthly factors of change (FC) of surface inflow (into HRU1), run-off (from HRU12) and modelled saturation levels are evaluated along with contributions of climate model and stochastic uncertainty for each future climate period (as described in Hirschberg et al., 2021).

3 | RESULTS

3.1 | RAMMS-calibrated debris-flow event catalogue

The RAMMS model calibration produced an event catalogue containing seven fully calibrated debris-flow events (Figure 2a–g, Table 1). Maximum flow depths and eroded volumes were accurately reproduced, while the observed hydrograph shape could be maintained along the flow path. The calibration values obtained for the RAMMS erosion proportionality factor $dz/d\tau_{cal}$ (indicating channel-bed erodibility), exhibit a statistically significant correlation with observed erodibility ($dz/d\tau_{obs}$), which was calculated from measured debris-flow front properties (Figure 2h, Table 1). Although the two parameters are not directly comparable because $dz/d\tau_{cal}$ incorporates the spatially distributed maximum shear stress while the eroded depth for $dz/d\tau_{obs}$ is scaled with local maximum shear stress measured at CD29, this finding indicates a physical foundation for the calibrated erodibility values.

The calibration results were particularly satisfactory for debris-flow events with a large depth, steep front, no roll-wave formation and no secondary surges (e.g., Events 1, 4, 10 and 15, Figure 2). For events with more complex hydrographs, the calibration process required additional assumptions, resulting in a higher level of uncertainty in the calibration parameters. For example, the hydrograph recorded for Event 12 showed strong oscillations due to roll waves after the front had passed (Figure 2e). Because these oscillations cannot be replicated with RAMMS, a 100-s moving average of the measurements was used as the basis for the input hydrograph (Appendix A.1, Figure A2 in the Supporting Information). In the case of Event 3, modifications of the input hydrograph (i.e., a 250-s delay in front arrival) were necessary to prevent the model output hydrograph from extreme frontal bulking (Figure 2b and Appendix A.1, Figure A2 in the Supporting Information). Although it is possible that the hydrograph shape evolves along the modelling reach, and the impact on the value of the erodibility parameter was found to be negligible, it is important to highlight that the procedure diverges from the conventional calibration method for this specific event. Furthermore, in this particular instance, the RAMMS model encounters numerical instabilities manifesting as stationary lateral waves.

3.2 | Water balance model calibration

The InfChan model's annual water balance demonstrates a notable decrease in surface run-off along the flow path, with only 20% of the incoming water run-off at the fan apex leaving the lowest modelled channel reach as surface run-off. Only larger discharge events reach the lower channel (Figure 3). The water losses in the form of infiltration (81% to 85% of annual surface inflow) predominantly drain to lower soil layers. Actual evaporation (203 mm a^{-1}) amounts to much smaller values than annual evapotranspiration reported in the Hydrological Atlas of Switzerland (2015). This discrepancy is anticipated because the InfChan model does not encompass any elements representing transpiration because the modelled area lacks vegetation, and water availability is limited. Mean annual precipitation sums directly on the channel surface (821 mm a^{-1}) correspond to only 3.0% of annual surface inflow from the headwaters.

The soil-specific parameters selected in the calibration procedure were generally in agreement with values reported in previous studies on hydraulic properties of sandy loam (Table 2). The model performance showed a strong dependence on the equilibrium infiltration rate f_c, and thus, the best-fit parameter value could easily be defined. The decay parameter k on the other hand could not be well

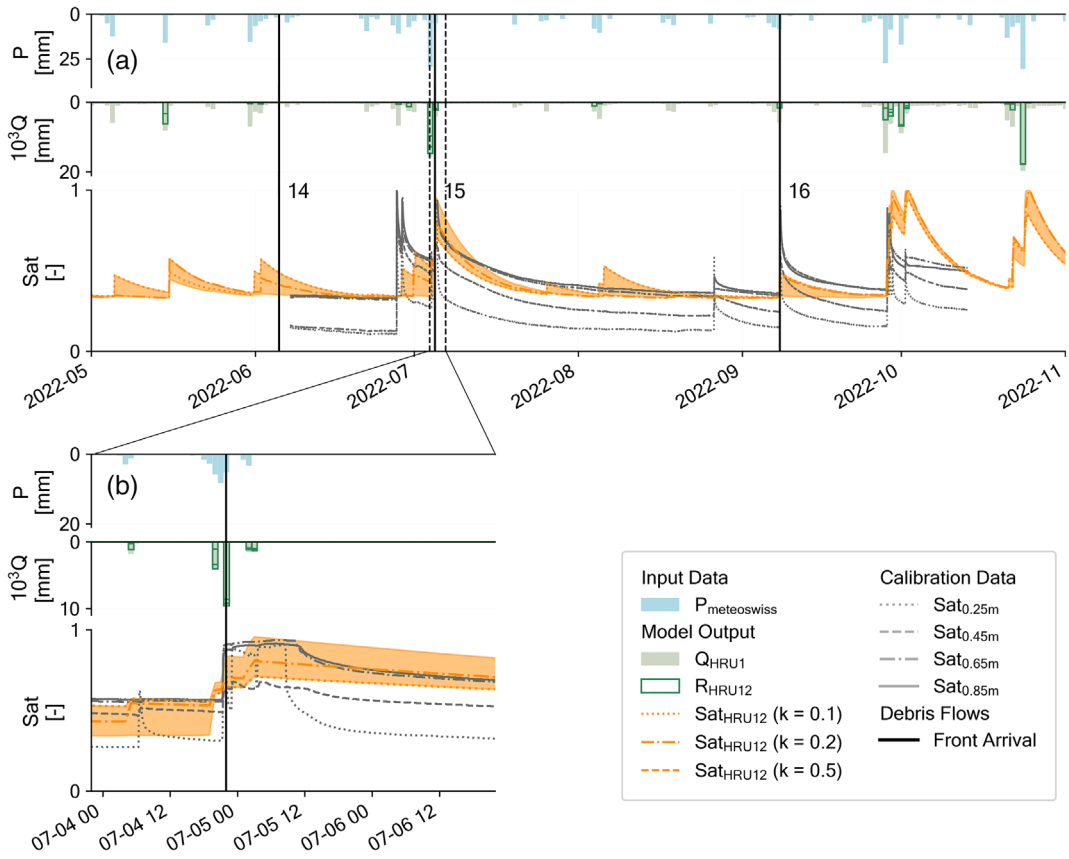

FIGURE 3 Time series of the debris-flow season of 2022 for precipitation (*P*), run-off (Q) and saturation level (*Sat*) (a) showing the InfChan model input (precipitation, $P_{meteoswiss}$) and the surface inflow generated by SedCas (Q_{HRU1}) at a daily time scale, along with an ensemble of saturation level time series (Sat_{HRU12}, orange shading) and daily surface run-off (R_{HRU12}) at the lowermost channel section, resulting from the infiltration model with different *k*-parameter values. Additionally, the soil moisture measurements on the channel bank at location SM28 at different depths are displayed. The numbered vertical black lines represent the front arrival of the respective debris-flow events (labelled with event ID). On the bottom graph (b), hourly data of the same variables are shown for Debris-Flow Event 15. [Color figure can be viewed at wileyonlinelibrary.com]

constrained by observed data because it only marginally influences model performance while still affecting the modelled saturation level. To account for InfChan's parameter uncertainty, the three best-performing model parametrizations with different *k* values were considered for further analysis (Figure 3). The resulting range of model uncertainty varied over time, with large deviations observed during active infiltration process, and relatively narrow value ranges during dry periods.

Overall, the time series of water content derived from the InfChan model ensemble was able to capture the most relevant hydrological behaviour observed at the Illgraben channel (Figure 3). At the seasonal scale, the number of flow impulses reaching the soil storage and the soil's drying rate after a wetting event show a satisfactory performance when compared with measured soil moisture data and observed flow frequencies (refer to Appendices A.3 and B.1 in the Supporting Information). At the event scale, the timing of the wetting front and the degree of saturation reached visually align with the soil moisture measurements (Figure 3b).

3.3 | Correlating erodibility and channel-bed saturation levels

The best predictive power for estimating the erodibility based on InfChan results for water content was found using a maximum soil storage parameter M_{max} of 1400 mm (Table 2). When excluding obvious outliers, the model results exhibited correlations that were (marginally) significant (as discussed in the subsequent section). Furthermore, selecting three model parametrizations (i.e., with varying *k* values, refer to Section 3.2) enhances the model's predictive capability compared with a single best-fit model and yields similar results as a model that considers five parametrizations. The selected model ensemble also demonstrates satisfactory agreement with soil moisture data measured at SM28 (Figure 3).

Both graphs display a considerable scatter of data points and some clear outliers (i.e., Events 3, 5, 11 and 12). When considering the different classes of debris flows (i.e., multi-surge, roll-wave-forming and gradual front), it is apparent that for single-surge events with a steep front (i.e., 'Debris Flows'), the calibrated erodibility (Figure 4a) is strongly correlated with modelled water content. Comparison with the results derived from the calibration of the Iverson et al. (2011) entrainment experiments (i.e., 'Flume Exp.') reveal a clear overlap with the catalogue of calibrated steep-front single-surge events recorded and modelled at Illgraben. Roll-wave forming events, however, do not align with the expected erodibility–saturation relationship. Note that the two Outlier Events 3 and 12 have also shown outlier behaviour in the RAMMS calibration procedure (Section 3.1). For the observed erodibility (Figure 4b), outliers and extreme erosive or depositional events (i.e., Events 7–9) exhibit complex flow dynamics (i.e., multiple surges, gradual fronts and roll waves). Furthermore, a (marginally)

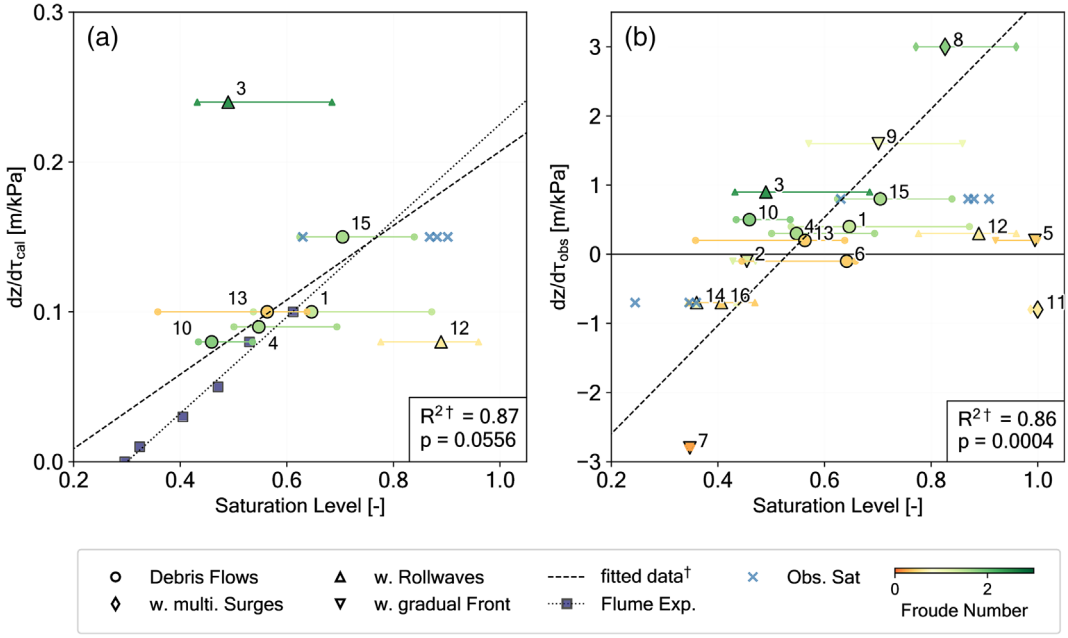

FIGURE 4 (a) RAMMS-calibrated ($dz/d\tau_{cal}$) and (b) observed ($dz/d\tau_{obs}$) erodibility plotted against modelled saturation levels along the flow path at the hour of debris-flow front arrival. On the left panel, additional data are plotted (i.e., measured water content on the channel bank [*Obs. Sat*] and RAMMS calibration results of the Iverson flume experiments [*Flume Exp.*]). The lines and smaller markers indicate the model uncertainty, the numbers indicate the event ID (refer to Table 1) and the dashed line marks the linear approximation to the plotted data. The *R* value indicates the Pearson correlation coefficient (†without Outlier Events 3, 5, 11 and 12) and its *p* value. Negative $dz/d\tau_{obs}$ values indicate events with net deposition. Please note that not all events were modelled with RAMMS and that $dz/d\tau_{cal}$ and $dz/d\tau_{obs}$ are not equivalent variables (Section 3.1). [Color figure can be viewed at wileyonlinelibrary.com]

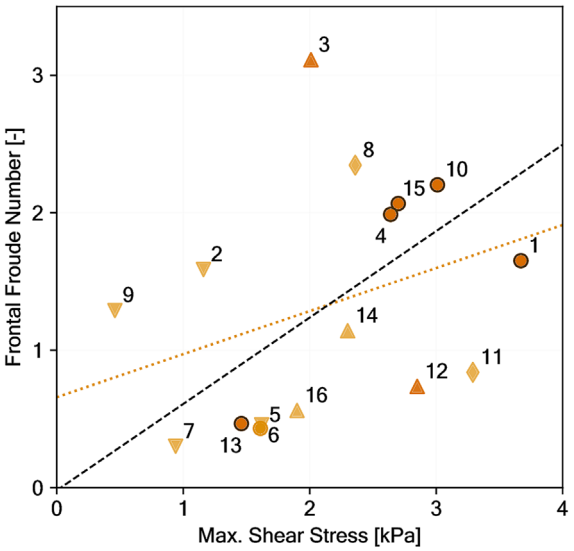

FIGURE 5 Maximum shear stress and frontal Froude number observed for the 16 events included in this study (Table 1). The linear regression line of the entire dataset and of the RAMMS-calibrated debris flows (without Outlier Events 3 and 12) separates the data points into shear stress dominated events and events dominated by inertial forces. [Color figure can be viewed at wileyonlinelibrary.com]

significant correlation between Froude number and channel-bed erodibility can be observed (calibrated: $R^2 = 0.69, p = 0.089$; observed: $R^2 = 0.60, p = 0.014$), while no dependence of the Froude number on saturation levels can be detected ($R^2 = -0.14, p = 0.607$).

Comparison of the maximum measured shear stress and the frontal Froude number (Figure 5) shows how, despite considerable scatter, there is a prevailing pattern of high Froude numbers (and hence large inertial forces within the flow) correlating with high shear stresses. By plotting the linear regression of the data points (encompassing both the complete dataset and only the well-calibrated events observed in Figure 4a), it becomes apparent that some events show increased Froude numbers even when shear forces are low (e.g., Event 3), whereas other events are dominated by shear forces (e.g., Events 11 and 12).

Antecedent rain sums (AR) have shown to be most predictive for channel erosion in Illgraben at a 3-h aggregation scale (de Haas et al., 2022). In fact, AR(3h) values have shown a positive correlation with calibrated and observed channel-bed erodibility (Appendix B.2, Figure B5 in the Supporting Information). The events with high antecedent water availability (i.e., Events 1, 3, 4 and 15) completely differ from the high water-content events predicted by InfChan, and antecedent precipitation does not correlate with modelled water content in the channel-bed ($R^2 = 0.005, p = 0.984$). However, the Froude number does significantly correlate with antecedent rain sums

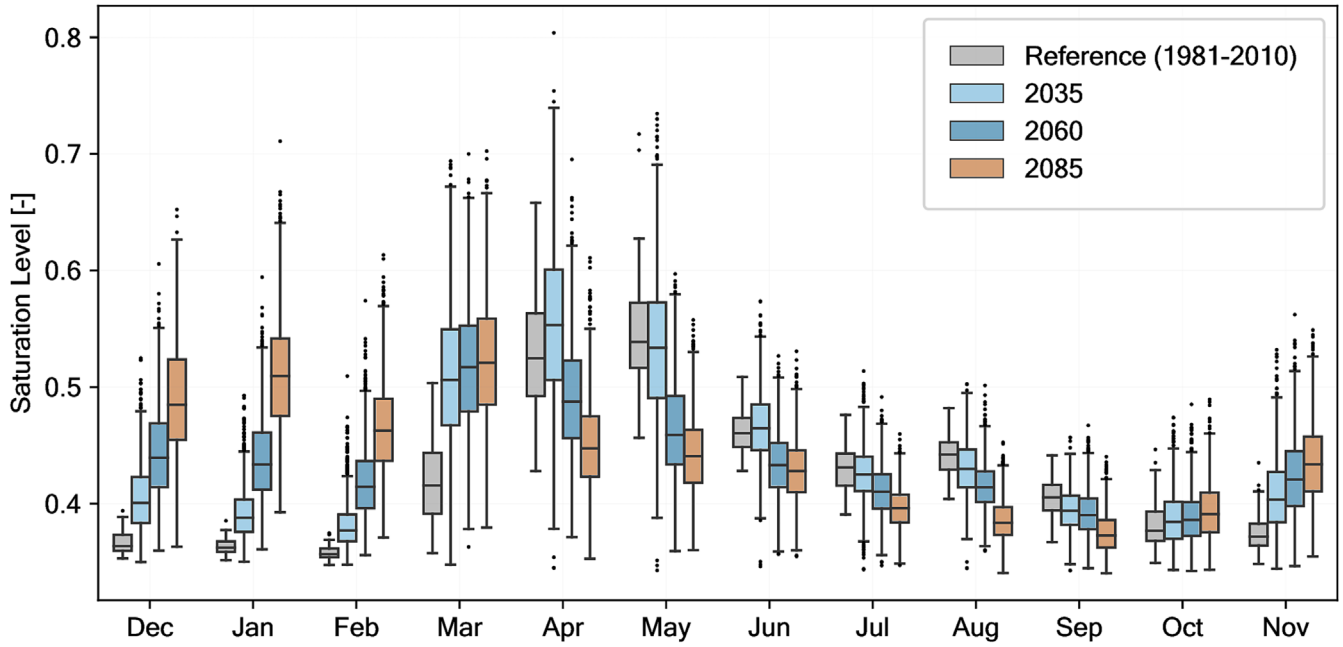

FIGURE 6 Long-term monthly median of modelled channel-bed saturation level at the lower reaches of Illgraben (HRU12) for current and future conditions. Water content is computed with the SedCas model, extended by the channel infiltration component InfChan and forced with the climate generated from AWE-GEN. Boxplots indicate the ensemble variability of long-term monthly median values for all AWE-GEN parameter sets (i.e., the box shows the quartiles, the middle line shows the median and the whiskers show the rest of the distribution, except for points that are determined to be outliers). Therefore, the Reference consists of 50 (one parameter set with 50 simulations) and the future scenarios of 1550 (30 + 1 parameter sets with 50 simulations each) data points. [Color figure can be viewed at wileyonlinelibrary.com]

($R^2 = 0.634, p = 0.008$), and total debris-flow volume shows significant correlation with Froude numbers ($R^2 = 0.742, p = 0.001$) and antecedent rain ($R^2 = 0.627, p = 0.009$; Appendix B.3, Figure B6 in the Supporting Information). Hence, debris flows preceded by larger amounts of precipitation tend to have large flow volumes, higher Froude numbers and more distinct flow fronts.

Any prediction of channel-bed erodibility based on channel-bed elevation previous to the event or the event's frontal bulk density was not possible, as data seemed to be uncorrelated. Furthermore, no discernible seasonal trend was evident in the dataset.

3.4 | Climate change impact on channel-bed moisture conditions

Changes in the hydrological regime forecasted for the RCP8.5 scenario greatly affect the monthly moisture conditions expected at the Illgraben channel bed (Figure 6). Peak values of water content, currently expected in late spring (i.e., April–May), continuously shift towards the winter months over the next few decades, resulting in substantial increases in water content from December to March. During the debris-flow season, which is currently from May to October, a steady decrease in moisture availability is expected (except for October), making it the season with the driest channel-bed conditions by the end of the century.

The changes in moisture conditions and surface run-off and the partitioning of climate model uncertainty and internal climate variability align with the results presented in Hirschberg et al. (2021) for the semi-distributed SedCas model (Appendix B.4, Figure B7 in the Supporting Information).

4 | DISCUSSION

4.1 | Predictability of channel-bed erodibility

For debris flows characterized by a single surge and a steep front, RAMMS showed good performance in reproducing key debris-flow characteristics. Thus, the event's erosivity (i.e., modelled shear stress) and the channel-bed erodibility ($dz/d\tau_{cal}$) could be separated. Under these circumstances, calibrated erodibility could explicitly be linked to modelled water-content values (Figure 4). This outcome supports the main assumption of this study that a higher bed water content results in higher bed pore pressures and consequently in larger entrainment quantities (Iverson et al., 2011). Additionally, high saturation levels in the channel bed increase the probability of bed liquefaction, further promoting entrainment (Roelofs et al.,2023).

The calibration of the flume experiments conducted by Iverson et al. (2011) show a similar relation between saturation level and erodibility. Notably, the data were derived from two fundamentally different sources: a large-scale flume experiment and a natural debris-flow basin with different characteristics (e.g., grain size distribution and channel slope). This indicates that a potential relationship between flow-path moisture conditions and channel-bed erodibility may be applicable to a wide range of conditions and at various locations.

However, for many events included in this analysis, flow dynamics could not be entirely reproduced (i.e., Events 3 and 12) or not modelled at all (i.e., Events 5, 8 and 9 and all depositional events). This makes the resulting erodibility values (calibrated and observed) dependent on additional factors other than channel-bed conditions. Thus, the variability in the erodibility parameters cannot be ascribed solely

to bed erodibility (e.g., channel-bed moisture conditions) but also depends on the erosive potential of the flow (i.e., erosivity).

4.2 | The influence of debris-flow erosivity on entrainment

For debris flows characterized by a more complex rheology, the hypothesized link between flow-path saturation level and bed erodibility could not be empirically supported. One explanation for this discrepancy is attributed to the limitation of the RAMMS erosion module, which exclusively considers shear forces in the simulation of debris-flow erosivity (Bartelt et al., 2013). However, the entrainment process is demonstrably influenced by other forces and flow mechanisms as well (Berger et al., 2011; Choi & Song, 2023; Roelofs et al., 2022).

The events producing less satisfactory results in the RAMMS simulation (i.e., Events 3 and 12) both display a clear pattern of roll-wave propagation starting shortly after the front arrival and possibly leading to substantial variation in the flow's erosivity (Figure 2b,e). The two events also deviate from the expected scaling of maximum shear stresses and flow inertial forces (i.e., the Froude numbers, Figure 5). The (marginally) significant correlation between Froude number and bed erodibility supports the notion that flow inertial forces do influence the entrainment process. As their effect on the erosive power of a debris flow is not reproducible in RAMMS, erosivity may be underpredicted for Event 3 (with its high velocity and high bulk density) and overpredicted for Event 12 (with its slow, muddy and viscous flow behaviour reportedly manifesting in relatively small normal-force fluctuations compared with shear forces de Haas et al., 2022). Thus, the channel-bed erodibility parameter $dz/d\tau$ needs to be corrected accordingly (i.e., reduced for Event 3, increased for Event 12), which results in a better alignment with the established saturation–erodibility relationship (Figure 4).

These findings indicate that the RAMMS model can replicate debris flows without roll waves and where inertial forces (i.e., the Froude number) scale with shear forces. For the remaining events (no. 3 and 12), it becomes difficult to quantify the influence of, and a possible relationship between, the two identified phenomena (i.e., roll-wave propagation and prevailing inertial forces). Either way, the calibration of RAMMS becomes more involved, necessitating additional data and effort to isolate the erodibility parameter and assess the influence of antecedent channel-bed saturation level.

The absence of a correlation between modelled water content and Froude number further strengthens the proposition that channel-bed erodibility and event erosivity are governed by separate mechanisms.

4.3 | Erosivity and water availability

In addition to the modelled bed water content immediately prior to the debris-flow occurrence, the antecedent precipitation conditions were considered, revealing a possible dependence of debris-flow erosivity on water availability in the headwaters.

Specifically, the 3-h antecedent rain sums correlate with erodibility values and with Froude numbers and total flow volume, while modelled flow-path saturation level seems to have no influence on Froude number and flow volume. This observation highlights the interplay between entrainment mechanisms taking place in the fan area (e.g., saturation-dependent erosion) and the headwaters. High water availability due to intense precipitation in the headwaters corresponds to a high initial transport capacity, leading to progressively higher shear forces and velocities as the debris flow mobilizes larger amounts of sediment along its flow path. Furthermore, high water availability can be expected to increase pore pressures within the flow masses, leading to a higher erosivity by influencing the transfer of interstitial fluid from the flow to the bed. However, this process also depends on the viscosity of the interstitial fluid, which in turn depends on the material composition of the debris flow (Roelofs et al.,2022).

The fact that modelled channel-bed water content does not correlate with 3-h antecedent rainfall sums could be attributed to the hydrological processes governing channel-bed moisture conditions (and hence increased entrainment), differing from those responsible for triggering the mass movements (and thus determining the debris flow's initial size). Alternatively, the discrepancy between modelled water content and the other parameters describing debris-flow behaviour can be ascribed to the inherent model and input data uncertainties.

4.4 | Quantification of channel-bed water content and underlying uncertainties

The calibrated values of the InfChan soil hydraulic parameters align with values reported in the literature (Table 2), and the model generally reproduces the expected hydrological properties on the seasonal and on the event scale (Figure 3). For instance, the model effectively captures the characteristics observed at ephemeral fan streams, with enhanced flow activity due to snow melt between March and May (Figure 6), and typically showing losing behaviour during transient and low discharge flows (Blackburn et al., 2021). The surface run-off component dominates the modelled water balance (Figure 3), making the direct impact of precipitation on the channel surface negligible.

Neither the SedCas hydrological module nor InfChan consider routing along the flow path of the torrent. This simplification is considered acceptable given the coarse temporal resolution selected for both models (1 h). Hence, the flow has enough time to propagate through the entire simulated catchment (Figure 1) within one time step. Furthermore, due to the implemented hourly resolution, the InfChan model might not be able to capture short-term infiltration processes, such as soil wetting due to sub-hourly intense precipitation events. However, correlating antecedent rain sums with debris-flow erodibility has shown that reducing the aggregation step below 3 h leads to a substantial decrease in predictive power (de Haas et al., 2022). Similarly, the storage volume yielding the best prediction for channel-bed erodibility indicates a memory effect active over multiple hours. Thus, the moisture conditions controlling the entrainment process are governed by long-term processes rather than instantaneous wetting and are dominated by run-off generation in the headwaters rather than direct impact of infiltrating precipitation. Short-term infiltration processes resulting from the interaction of debris flows with the channel bed (e.g., exfiltration of interstitial fluid Roelofs et al.,

2022) were attributed to flow conditions (erosivity) rather than to the antecedent state of the channel bed.

The development of the presented water balance model was hampered by limited data availability. The data used to constrain the infiltration parameters were not continuous, which prevented the application of established calibration approaches. In addition, for the most relevant input data used in the model (precipitation *P*), measurements may deviate from local patterns due to the considerable geographical distance and different orientation between Montana and the Illgraben sites. Thus, reliable precipitation measurements and more information on the surface and subsurface hydrological processes within the Illgraben fan area can be expected to improve model performance.

4.5 | Climate change impacts on debris-flow entrainment

We used RCP8.5 climate change scenarios to investigate future channel-bed moisture conditions, which can be complemented with predicted climate change impacts on debris-flow triggering (Hirschberg et al.,2021) to discuss future trends in debris-flow volumes. Although less extreme emission scenarios may be considered for decision-making, RCP8.5 is the most suitable one for exploring climate risks because it covers a large range of changes (Tollefson, 2020). Furthermore, due to internal climate variability, changes are often only considerable for the end of the century, even with this extreme scenario.

Future bed water-content conditions along the flow path are expected to substantially increase during winter and early spring driven by more frequent liquid precipitation and an earlier onset of the snow-melt season. During late spring and summer months, a decline in channel water content is expected, which can be attributed to the shifting pattern of snow melt and the reduced amounts of summer precipitation (Hirschberg et al., 2021). The water-content threshold at which pronounced erosive behaviour becomes dominant is estimated to be approximately 0.45 saturation level as in Figure 4. The predicted decrease in water content below this threshold during the summer months might result in less entrainment and more deposition. Conversely, winter months can be expected to exceed the erodibility threshold.

Water discharges large enough to trigger debris flows are expected to become more frequent in future climate. However, debris-flow dynamics depend on sediment availability as well. In Hirschberg et al. (2021), where only frost cracking is used as hillslope sediment production process, a decrease in sediment availability is predicted, especially in summer and autumn. Under this assumption, the probability of large debris flows occurring in the summer is expected to decrease. However, if other hillslope processes continue to produce sediment, such as a large rock slide like that of 1961 (Hürlimann et al., 2003), or if sediment accumulates in the channel due to drier channel-bed conditions, the potential for more catastrophic debris flows, channel overtopping and avulsion during the summer months may increase. Furthermore, the combination of increased triggering probability and wetter conditions may lead to larger event volumes earlier in the year, potentially challenging current mitigation strategies.

4.6 | Implications for practical applications

The presented modelling framework could be used to develop practical application guidelines on how practitioners deal with the problem of entrainment in hazard and mitigation assessments. By running long-term hydrological simulations, probabilities of channel wetness can be calculated and considered in risk analyses. This may become increasingly relevant as, with ongoing climate change, wetness conditions are expected to change considerably and therefore affect entrainment and mobility. Furthermore, permafrost-related processes could be included in the presented framework to predict potential future changes in erodibility of the affected headwater areas.

Before applying the proposed framework to practical problems, it is important to test it at other sites (e.g., the Bondo debris-flow event of 2017 Walter et al., 2020). This would extend the dataset and increase the confidence in the developed relationship between erodibility and water content.

The presented results showed that the framework works well for steep-front single-surge events. This type of debris flow generally corresponds to the flow behaviour assumed for practical applications where detailed flow-depth measurements are not available but are usually approximated by a three-point hydrograph (Bartelt et al., 2013). Hence, the presented relationship between entrainment and flow-path moisture conditions can be embedded in existing practices without much adaptation.

However, more complex flow types included in the presented dataset could not be integrated into the main premise of this study, as flow propagation and entrainment follow more complex mechanisms. To advance debris-flow entrainment modelling, gaining a physical understanding of the underlying mechanisms is crucial. Furthermore, flow patterns such as roll waves need to be integrated in debris-flow models to better separate the effects of flow erosivity from channel-bed erodibility. The recent development of a two-phase version of RAMMS (Meyrat et al., 2022) or other multi-phase models (e.g., George & Iverson, 2011; Mergili et al., 2017) present a promising opportunity for a more comprehensive examination of entrainment and flow mechanisms, as well as the interactions with pore water in the flow and channel bed. Nevertheless, because their application is limited to scientific contexts, the insights acquired in debris-flow physical processes and their simulation would require translation into a more practical model.

5 | CONCLUSIONS

We developed a framework for estimating debris-flow entrainment based on the shear stress of the flow and the wetness conditions of the channel bed. The RAMMS debris-flow entrainment model generated satisfactory simulations of flow characteristics and the entrained volumes for erosive debris-flow events characterized by single surges with steep fronts. Likewise, when coupled with hydrological models (SedCas and InfChan), this approach enabled accurate prediction of channel-bed erodibility, albeit only for the events with simple hydrograph shapes. The resulting correlation between independently calculated water content and calibrated flow-path erodibility demonstrates good agreement with both data derived from flume experiments and field measurements, providing a solid basis for the formulation of

practical application guidelines and the implementation of probability-based risk assessment.

The presented framework is limited to single-surge events, as events exhibiting more complex flow behaviour involve more intricate interactions between the debris-flow body and the flow path. Consequently, the erosional patterns for such events could not be explained. Further research would be beneficial to understand the underlying physical processes and to develop a practical model that incorporates these additional flow and erosion mechanisms (e.g., roll-wave generation and deposition process) before investigating the role of flow-path saturation conditions in these events.

Finally, the framework allowed for an investigation of future trends in channel-bed saturation level and erodibility. We found that under an extreme climate change scenario, future conditions in the Illgraben catchment favour more substantial and erosive debris flows in the winter and early spring, while dampening debris entrainment during the main debris-flow season from May to October. These findings provide an opportunity to incorporate the impacts of climate change into the assessment of future debris-flow-related risks and, consequently, into the formulation of mitigation strategies.

6 | AUTHOR CONTRIBUTIONS

Conceptualization: All authors. *Funding acquisition*: Perry Bartelt and Brian W. McArdell. *Methodology*: Anna Lena Könz, Jacob Hirschberg, Brian W. McArdell, Tjalling de Haas and Peter Molnar. *Investigation*: Anna Lena Könz, Jacob Hirschberg, Brian W. McArdell, Benjamin B. Mirus and Tjalling de Haas. *Software*: Jacob Hirschberg, Anna Lena Könz and Brian W. McArdell. *Supervision*: Jacob Hirschberg, Brian W. McArdell and Peter Molnar. *Writing—initial draft*: Anna Lena Könz and Jacob Hirschberg. *Writing—reviewing and editing*: All authors.

ACKNOWLEDGEMENTS

This study was partly funded by the WSL research programme Climate Change Impacts on Alpine Mass Movements (CCAMM). We thank D. George (USGS) and A. Badoux (WSL) for technical review and feedback, S. Boss and C. Graf (WSL) for technical assistance with debris-flow data collection and D. Bolliger (GEOTEST) for sharing the RAMMS calibration results.

DISCLAIMER

Any use of trade, firm or product names is for descriptive purposes only and does not imply endorsement by the US government.

DATA AVAILABILITY STATEMENT

Debris-flow data are available at https://www.doi.org/10.16904/envidat.173, topographic data are available at https://doi.org/10.3389/frsen.2021.626810 and soil moisture data are available at https://www.doi.org/10.16904/envidat.489. Observed climate data and climate scenarios were provided by the Swiss Federal Office of Meteorology (MeteoSwiss) and the National Center for Climate Services (NCCS), respectively, and are available for research purposes.

ORCID

Anna Lena Könz https://orcid.org/0000-0002-6339-3169
Jacob Hirschberg https://orcid.org/0000-0002-0348-7921
Brian W. McArdell https://orcid.org/0000-0002-5322-8741
Benjamin B. Mirus https://orcid.org/0000-0001-5550-014X
Tjalling de Haas https://orcid.org/0000-0001-8949-3929
Perry Bartelt https://orcid.org/0000-0001-7208-175X
Peter Molnar https://orcid.org/0000-0001-6437-4931

REFERENCES

Aaron, J. & McDougall, S. (2019) Rock avalanche mobility: the role of path material. *Engineering Geology*, 257, 105126. Available from: https://linkinghub.elsevier.com/retrieve/pii/S0013795218319240

Badoux, A., Andres, N., Techel, F. & Hegg, C. (2016) Natural hazard fatalities in Switzerland from 1946 to 2015. *Natural Hazards and Earth System Sciences*, 16(12), 2747–2768. Available from: https://nhess.copernicus.org/articles/16/2747/2016/

Baggio, T., Mergili, M. & D'Agostino, V. (2021) Advances in the simulation of debris flow erosion: the case study of the Rio Gere (Italy) event of the 4th August 2017. *Geomorphology*, 381, 107664. Available from: https://linkinghub.elsevier.com/retrieve/pii/S0169555X21000726

Bartelt, P., Buehler, Y., Christen, M., Deubelbeiss, Y., Graf, C. & McArdell, B.W. (2013) *RAMMS—rapid mass movement simulation, a modeling system for debris flows in research and practice, user manual v1.5, debris flow, manuscript update: 31 January 2013*. Davos, Switzerland: WSL Institute for Snow and Avalanche Research SLF, Davos. Available from: http://ramms.slf.ch/ramms/downloads/RAMMS_DBF_Manual.pdf

Bennett, G.L., Molnar, P., McArdell, B.W. & Burlando, P. (2014) A probabilistic sediment cascade model of sediment transfer in the Illgraben. *Water Resources Research*, 50(2), 1225–1244. Available from: http://doi.wiley.com/10.1002/2013WR013806

Berger, C., McArdell, B.W. & Schlunegger, F. (2011) Direct measurement of channel erosion by debris flows, Illgraben, Switzerland. *Journal of Geophysical Research: Earth Surface* 116(F1), F01002. Available from: https://agupubs.onlinelibrary.wiley.com/doi/abs/10.1029/2010JF001722

Berger, C., McArdell, B.W. & Schlunegger, F. (2011) Sediment transfer patterns at the Illgraben catchment, Switzerland: implications for the time scales of debris flow activities. *Geomorphology*, 125(3), 421–432. Available from: https://linkinghub.elsevier.com/retrieve/pii/S0169555X10004484

Blackburn, J., Comte, J.C., Foster, G. & Gibbins, C. (2021) Hydrogeological controls on the flow regime of an ephemeral temperate stream flowing across an alluvial fan. *Journal of Hydrology*, 595, 125994. Available from: https://linkinghub.elsevier.com/retrieve/pii/S002216942100041X

Bolliger, D., Schlunegger, F. & McArdell, B.W. (2024) Comparison of debris flow observations, including fine-sediment grain size and composition and runout model results, at the Illgraben, Swiss Alps. *Natural Hazards and Earth System Sciences*, 24, 1035–1049.

C., B. (1933) Irrigation principles and practices. *Nature*, 132(3323), 47–47. Available from: https://doi.org/10.1038/132047a0

CH2018 (2018) *CH2018—climate scenarios for Switzerland, Technical report*. Zurich: National Centre for Climate Services.

Choi, C.E. & Song, P. (2023) New unsaturated erosion model for landslide: effects of flow particle size and debunking the importance of frictional stress. *Engineering Geology*, 315, 107024. Available from: https://linkinghub.elsevier.com/retrieve/pii/S0013795223000418

Christen, M., Kowalski, J. & Bartelt, P. (2010) RAMMS: numerical simulation of dense snow avalanches in three-dimensional terrain. *Cold Regions Science and Technology*, 63(1-2), 1–14. Available from: https://linkinghub.elsevier.com/retrieve/pii/S0165232X10000844

de Haas, T., McArdell, B.W., Nijland, W., Åberg, A.S., Hirschberg, J. & Huguenin, P. (2022) Flow and bed conditions jointly control debris-flow erosion and bulking. *Geophysical Research Letters*, 49(10), e2021GL097611. Available from: https://onlinelibrary.wiley.com/doi/10.1029/2021GL097611

de Haas, T., Nijland, W., de Jong, S.M. & McArdell, B.W. (2020) How memory effects, check dams, and channel geometry control erosion and deposition by debris flows. *Scientific Reports*, 10(1), 14024. Available from: https://www.nature.com/articles/s41598-020-71016-8

Dietrich, A. & Krautblatter, M. (2019) Deciphering controls for debris-flow erosion derived from a LiDAR-recorded extreme event and a

calibrated numerical model (Roßbichelbach, Germany). *Earth Surface Processes and Landforms*, 44(6), 1346–1361. Available from: https://onlinelibrary.wiley.com/doi/10.1002/esp.4578

Dowling, C.A. & Santi, P.M. (2014) Debris flows and their toll on human life: a global analysis of debris-flow fatalities from 1950 to 2011. *Natural Hazards*, 71(1), 203–227. Available from: http://link.springer.com/10.1007/s11069-013-0907-4

Fatichi, S., Ivanov, V.Y. & Caporali, E. (2011) Simulation of future climate scenarios with a weather generator. *Advances in Water Resources*, 34(4), 448–467. Available from: https://linkinghub.elsevier.com/retrieve/pii/S0309170811000042

Fawcett, T. (2006) An introduction to ROC analysis. *Pattern Recognition Letters*, 27(8), 861–874. Available from: https://linkinghub.elsevier.com/retrieve/pii/S016786550500303X

Frank, F., McArdell, B.W., Huggel, C. & Vieli, A. (2015) The importance of entrainment and bulking on debris flow runout modeling: examples from the Swiss Alps. *Natural Hazards and Earth System Sciences*, 15(11), 2569–2583. Available from: https://nhess.copernicus.org/articles/15/2569/2015/

Frank, F., McArdell, B.W., Oggier, N., Baer, P., Christen, M. & Vieli, A. (2017) Debris-flow modeling at Meretschibach and Bondasca catchments, Switzerland: sensitivity testing of field-data-based entrainment model. *Natural Hazards and Earth System Sciences*, 17(5), 801–815. Available from: https://nhess.copernicus.org/articles/17/801/2017/

Gariano, S.L. & Guzzetti, F. (2016) Landslides in a changing climate. *Earth-Science Reviews*, 162, 227–252 en. Available from: https://linkinghub.elsevier.com/retrieve/pii/S0012825216302458

George, D.L. & Iverson, R.M. (2011) A two-phase debris-flow model that includes coupled evolution of volume fractions, granular dilatancy, and pore-fluid pressure. *Italian Journal of Engineering Geology and Environment*, 415–424. Available from: https://doi.org/10.4408/IJEGE.2011-03.B-047

Hirschberg, J., Badoux, A., McArdell, B.W., Leonarduzzi, E. & Molnar, P. (2021) Evaluating methods for debris-flow prediction based on rainfall in an Alpine catchment. *Natural Hazards and Earth System Sciences*, 21(9), 2773–2789. Available from: https://nhess.copernicus.org/articles/21/2773/2021/

Hirschberg, J., Fatichi, S., Bennett, G.L., McArdell, B.W., Peleg, N., Lane, S.N., Schlunegger, F. & Molnar, P. (2021) Climate change impacts on sediment yield and debris-flow activity in an Alpine catchment. *Journal of Geophysical Research: Earth Surface*, 126(1), e2020JF005739. Available from: https://onlinelibrary.wiley.com/doi/10.1029/2020JF005739

Hirschberg, J., McArdell, B.W., Badoux, A. & Molnar, P. (2019) Analysis of rainfall and runoff for debris flows at Illgraben catchment, Switzerland, 7th International Conference on Debris-Flow Hazard Mitigation. Philadelphia: Association of Environmental and Engineering Geologists.

Horton, R.E. (1939) Analysis of runoff-plat experiments with varying infiltration-capacity. *Eos, Transactions American Geophysical Union*, 20, 693–711.

Hungr, O. & McDougall, S. (2009) Two numerical models for landslide dynamic analysis. *Computers & Geosciences*, 35(5), 978–992. Available from: https://linkinghub.elsevier.com/retrieve/pii/S0098300408000289

Hürlimann, M., Rickenmann, D. & Graf, C. (2003) Field and monitoring data of debris-flow events in the Swiss Alps. *Canadian Geotechnical Journal*, 40(1), 161–175. Available from: https://doi.org/10.1139/t02-087

Hussin, H.Y., Quan Luna, B., van Westen, C. J., Christen, M., Malet, J.-P. & van Asch, T. W. J. (2012) Parameterization of a numerical 2-D debris flow model with entrainment: a case study of the Faucon catchment, Southern French Alps. *Natural Hazards and Earth System Sciences*, 12(10), 3075–3090. Available from: https://nhess.copernicus.org/articles/12/3075/2012/

Hydrological Atlas of Switzerland (2015) Mean precipitation [data set]. Available from: https://hydrologicalatlas.ch. Accessed: 2023-03-30.

Iverson, R.M., Reid, M.E., Logan, M., LaHusen, R.G., Godt, J.W. & Griswold, J.P. (2011) Positive feedback and momentum growth during debris-flow entrainment of wet bed sediment. *Nature Geoscience*, 4(2), 116–121. Available from: http://www.nature.com/articles/ngeo1040

Jakob, M. & Hungr, O. (2005) *Debris-flow hazards and related phenomena*. Berlin, Heidelberg: Springer.

Kaitna, R., Prenner, D., Switanek, M., Maraun, D., Stoffel, M. & Hrachowitz, M. (2023) Changes of hydro-meteorological trigger conditions for debris flows in a future Alpine climate. *Science of The Total Environment*, 872, 162227. Available from: https://linkinghub.elsevier.com/retrieve/pii/S0048969723008434

Lee, S., An, H., Kim, M., Lee, G. & Shin, H. (2022) Evaluation of different erosion-entrainment models in debris-flow simulation. *Landslides*, 19(9), 2075–2090. Available from: https://link.springer.com/10.1007/s10346-022-01901-y

Lichtenhahn, C. (1971) Zwei Betonmauern: Die Geschieberückhaltesperre am Illgraben [Wallis] und die Staumauer des Hochwasserschutzbeckens an der Orlegna im Bergell [Graubünden], Internationales Symposium Interpraevent, Villach, Austria: F.f.v. Hochwasserbekämpfung, Vol. 451–456 en.

McArdell, B.W. (2016) Field measurements of forces in debris flows at the Illgraben: implications for channel-bed erosion. *International Journal of Erosion Control Engineering*, 9(4), 194–198. Available from: https://www.jstage.jst.go.jp/article/ijece/9/4/9_194/_article

McArdell, B.W., Bartelt, P. & Kowalski, J. (2007) Field observations of basal forces and fluid pore pressure in a debris flow. *Geophysical Research Letters*, 34(7), L07406. Available from: http://doi.wiley.com/10.1029/2006GL029183

McArdell, B.W., Hirschberg, J., Graf, C., Boss, S. & Badoux, A. (2023) *Illgraben debris-flow characteristics 2019-2022*. Birmensdorf, Switzerland: EnviDat. Available from: https://www.envidat.ch/dataset/illgraben-debris-flow-characteristics-2019-2022

McCoy, S.W., Kean, J.W., Coe, J.A., Tucker, G.E., Staley, D.M. & Wasklewicz, T.A. (2012) Sediment entrainment by debris flows: in situ measurements from the headwaters of a steep catchment. *Journal of Geophysical Research: Earth Surface* 117(F3), F03016. Available from: http://doi.wiley.com/10.1029/2011JF002278

Meijer, N. C. J.M. (2019) Erosional forces in the Meretschibach and Illgraben: characterisation of soil processes in active debris flow catchments. Master Thesis, Wageningen University, Soil Geography and Landscape Group, Wageningen, Netherlands.

Mergili, M., Fischer, J.-T., Krenn, J. & Pudasaini, S.P. (2017) r.avaflow v1, an advanced open-source computational framework for the propagation and interaction of two-phase mass flows. *Geoscientific Model Development*, 10(2), 553–569. Available from: https://gmd.copernicus.org/articles/10/553/2017/

Meyrat, G., McArdell, B., Ivanova, K., Müller, C. & Bartelt, P. (2022) A dilatant, two-layer debris flow model validated by flow density measurements at the Swiss illgraben test site. *Landslides*, 19(2), 265–276. Available from: https://link.springer.com/10.1007/s10346-021-01733-2

Prochaska, A.B., Santi, P.M. & Higgins, J.D. (2008) Debris basin and deflection berm design for fire-related debris-flow mitigation. *Environmental & Engineering Geoscience*, 14(4), 297–313. Available from: https://doi.org/10.2113/gseegeosci.14.4.297

Quinlan, E., Gibbins, C.N., Batalla, R.J. & Vericat, D. (2015) Impacts of small scale flow regulation on sediment dynamics in an ecologically important upland river. *Environmental Management*, 55(3), 671–686. Available from: http://link.springer.com/10.1007/s00267-014-0423-7

Reid, M.E., Coe, J.A. & Brien, D.L. (2016) Forecasting inundation from debris flows that grow volumetrically during travel, with application to the Oregon Coast Range, USA. *Geomorphology*, 273, 396–411. Available from: https://www.sciencedirect.com/science/article/pii/S0169555X16306638

Roelofs, L., Colucci, P. & de Haas, T. (2022) How debris-flow composition affects bed erosion quantity and mechanisms: an experimental assessment. *Earth Surface Processes and Landforms*, 47(8), 2151–2169. Available from: https://onlinelibrary.wiley.com/doi/10.1002/esp.5369

Roelofs, L., Nota, E.W., Flipsen, T. C.W., Colucci, P. & De Haas, T. (2023) How bed composition affects erosion by debris flows—an

experimental assessment. *Geophysical Research Letters*, 50(14), e2023GL103294. Available from: https://agupubs.onlinelibrary.wiley.com/doi/10.1029/2023GL103294

Rossman, L.A. & Huber, W.C. (2016) Storm Water Management Model reference manual volume I—hydrology (revised). In EPA/600/R-15/162A, United States Environmental Protection Agency. Cincinnati, Ohio.

Sassa, K. & Wang, G.H. (2005) Mechanism of landslide-triggered debris flows: liquefaction phenomena due to the undrained loading of torrent deposits. In *Debris-flow hazards and related phenomena*. Berlin, Heidelberg: Springer, pp. 80–104.

Schürch, P., Densmore, A.L., Rosser, N.J. & McArdell, B.W. (2011) Dynamic controls on erosion and deposition on debris-flow fans. *Geology*, 39(9), 827–830. Available from: https://doi.org/10.1130/G32103.1

Tollefson, J. (2020) How hot will Earth get by 2100? *Nature*, 580(7804), 443–445. Available from: https://doi.org/10.1038/d41586-020-01125-x

Walter, F., Amann, F., Kos, A., Kenner, R., Phillips, M., de Preux, A., Huss, M., Tognacca, C., Clinton, J., Diehl, T. & Bonanomi, Y. (2020) Direct observations of a three million cubic meter rock-slope collapse with almost immediate initiation of ensuing debris flows. *Geomorphology*, 351, 106933 Available from: https://linkinghub.elsevier.com/retrieve/pii/S0169555X19304246

Wang, N. & Chu, X. (2020) Revised Horton model for event and continuous simulations of infiltration. *Journal of Hydrology*, 589, 125215. Available from: https://linkinghub.elsevier.com/retrieve/pii/S0022169420306752

Zheng, H., Shi, Z., Hanley, K.J., Zhou, Y. & Hu, X. (2023) Pore pressure evolution in bed sediment overridden by debris flow: a general formulation. *Earth Surface Processes and Landforms*, 48(6), 1188–1201. Available from: https://onlinelibrary.wiley.com/doi/abs/10.1002/esp.5542

SUPPORTING INFORMATION

Additional supporting information can be found online in the Supporting Information section at the end of this article.

How to cite this article: Könz, A.L., Hirschberg, J., McArdell, B.W., Mirus, B.B., de Haas, T., Bartelt, P. et al. (2024) Debris-flow entrainment modelling under climate change: Considering antecedent moisture conditions along the flow path. *Earth Surface Processes and Landforms*, 49(10), 2950–2964. Available from: https://doi.org/10.1002/esp.5868